Supplementary Information for

Cold-denaturation of a protein dimer monitored at atomic resolution

Mariusz Jaremko[1,2,6], Łukasz Jaremko[1,3,6], Hai-Young Kim[1], Min-Kyu Cho[1], Charles D. Schwieters[4], Karin Giller[1], Stefan Becker[1], Markus Zweckstetter[1,5,*]

[1] Department for NMR-based Structural Biology, Max Planck Institute for Biophysical Chemistry, 37077 Göttingen, Germany;

[2] Institute of Biochemistry and Biophysics, Polish Academy of Sciences, Pawińskiego 5A, 02-106 Warsaw, Poland;

[3] Faculty of Chemistry, Warsaw University, Pasteura 1, 02-093, Warsaw, Poland

[4] Division of Computational Bioscience, Building 12A, Center for Information Technology, National Institutes of Health, Bethesda, Maryland 20892-5624, USA.

[5] German Center for Neurodegenerative Diseases (DZNE), 37077 Göttingen, Germany.

[6] The authors contributed equally.

* To whom correspondence should be addressed. E-mail: Markus.Zweckstetter@dzne.de

Supplementary Results

a)
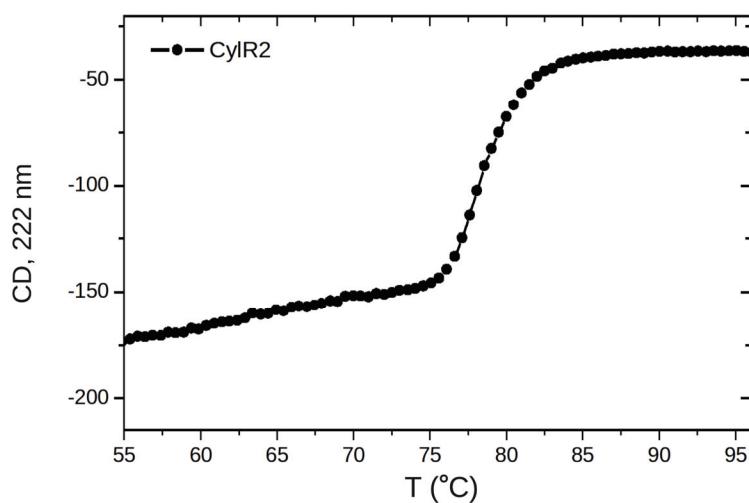
b)
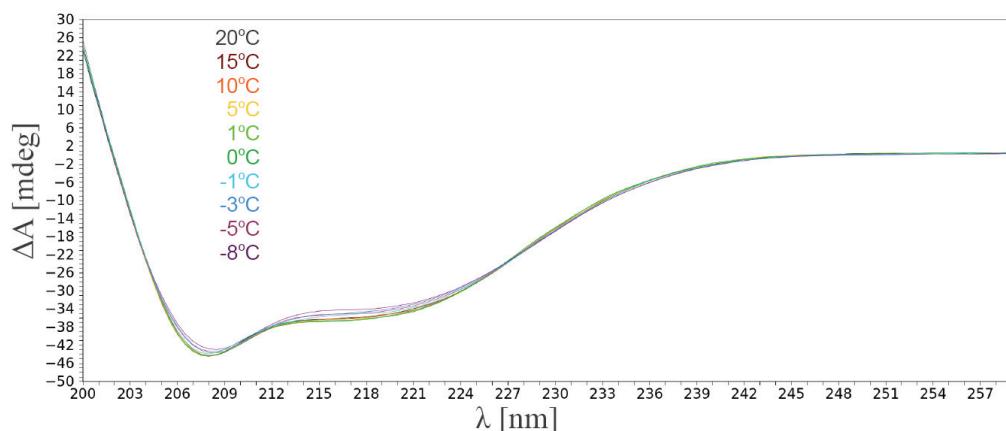
Supplementary Fig. 1. Analysis of secondary structure of CylR2 by circular dichroism. (a) Melting curve of CylR2 monitored at 222 nm (from a single measurement). The midpoint of heat denaturation is 77.5 °C. (**b**) Influence of decreasing temperatures. Below 0 °C small changes were observed at 208 nm and 214-220 nm consistent with the solved 3D structures (**Fig. 4**) that revealed the destabilization of the short (6 residues) terminal β-sheet with decreasing temperatures while the helical structure was preserved. Temperatures below -8 °C could not be reached due to limited stability of the CD instrument.

a)

```
25°C – NH
MIINNLKLIREKKKISQSELAALLEVSRQTINGIEKNKYNPSLQLALKIAYYLNTPLEDIFQWQPE
1         10        20        30        40        50        60

-3°C
MIINNLKLIREKKKISQSELAALLEVSRQTINGIEKNKYNPSLQLALKIAYYLNTPLEDIFQWQPE
1         10        20        30        40        50        60

-7°C
MIINNLKLIREKKKISQSELAALLEVSRQTINGIEKNKYNPSLQLALKIAYYLNTPLEDIFQWQPE
1         10        20        30        40        50        60

-11°C
MIINNLKLIREKKKISQSELAALLEVSRQTINGIEKNKYNPSLQLALKIAYYLNTPLEDIFQWQPE
1         10        20        30        40        50        60

-14°C
MIINNLKLIREKKKISQSELAALLEVSRQTINGIEKNKYNPSLQLALKIAYYLNTPLEDIFQWQPE
1         10        20        30        40        50        60

-16°C
MIINNLKLIREKKKISQSELAALLEVSRQTINGIEKNKYNPSLQLALKIAYYLNTPLEDIFQWQPE
1         10        20        30        40        50        60
```

β1   α1   α2   α3   α4   α5   β2

b)

```
25°C – Cα
MIINNLKLIREKKKISQSELAALLEVSRQTINGIEKNKYNPSLQLALKIAYYLNTPLEDIFQWQPE
1         10        20        30        40        50        60

-3°C
MIINNLKLIREKKKISQSELAALLEVSRQTINGIEKNKYNPSLQLALKIAYYLNTPLEDIFQWQPE
1         10        20        30        40        50        60

-7°C
MIINNLKLIREKKKISQSELAALLEVSRQTINGIEKNKYNPSLQLALKIAYYLNTPLEDIFQWQPE
1         10        20        30        40        50        60

-11°C
MIINNLKLIREKKKISQSELAALLEVSRQTINGIEKNKYNPSLQLALKIAYYLNTPLEDIFQWQPE
1         10        20        30        40        50        60

-14°C
MIINNLKLIREKKKISQSELAALLEVSRQTINGIEKNKYNPSLQLALKIAYYLNTPLEDIFQWQPE
1         10        20        30        40        50        60

-16°C
MIINNLKLIREKKKISQSELAALLEVSRQTINGIEKNKYNPSLQLALKIAYYLNTPLEDIFQWQPE
1         10        20        30        40        50        60
```

β1   α1   α2   α3   α4   α5   β2

Supplementary Fig. 2. Graphical representation of backbone ^{15}N-^{1}H (**a**) and ^{15}C$^{\alpha}$-^{1}H$^{\alpha}$ (**b**) cross-peaks that are no longer observable at decreasing temperatures.
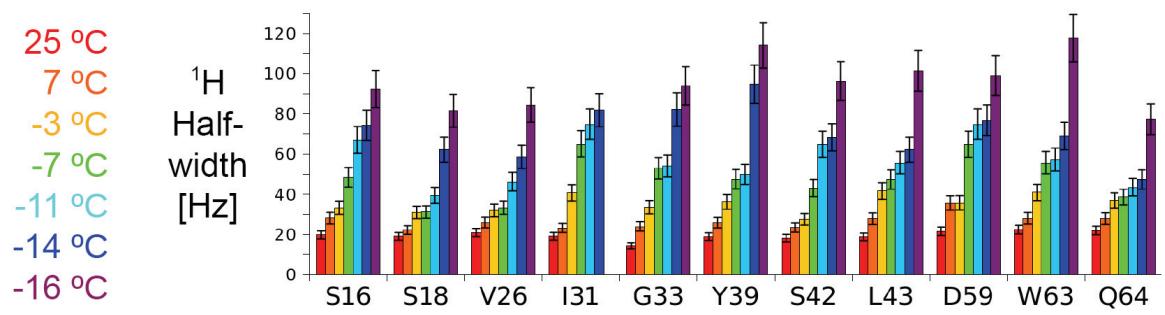
Supplementary Fig. 3. Increase in amide proton line widths at low temperatures due to the interconversion between different conformations at an intermediate exchange rate.
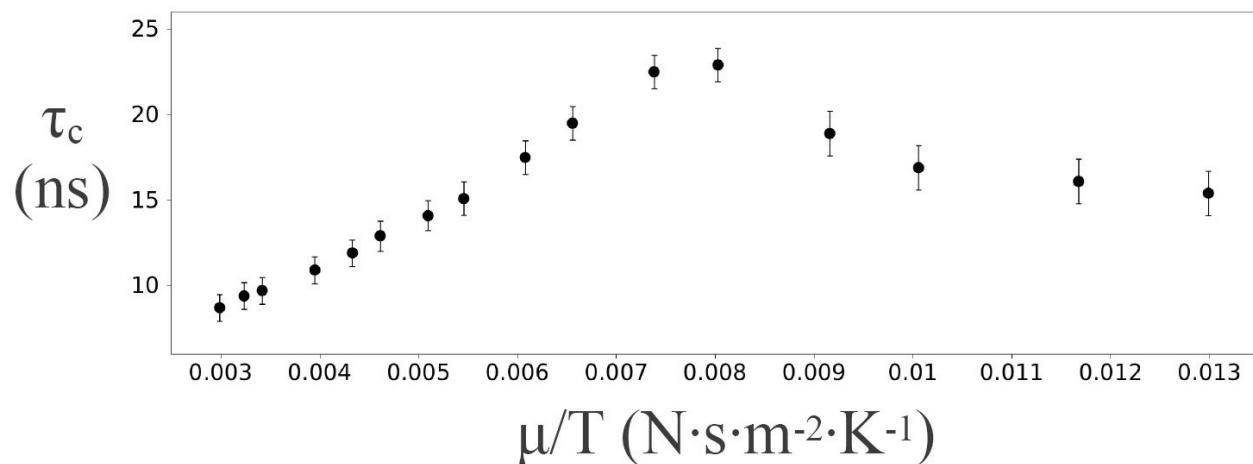
Supplementary Fig. 4. Relation between the global correlation time of CylR2, τ_c, and the dynamic viscosity of water $\eta(T)$ divided by the temperature of the measurement. Values of the dynamic viscosity of water were taken from http://www.engineeringtoolbox.com/water-dynamic-kinematic-viscosity-d_596.html and Hallett [1].
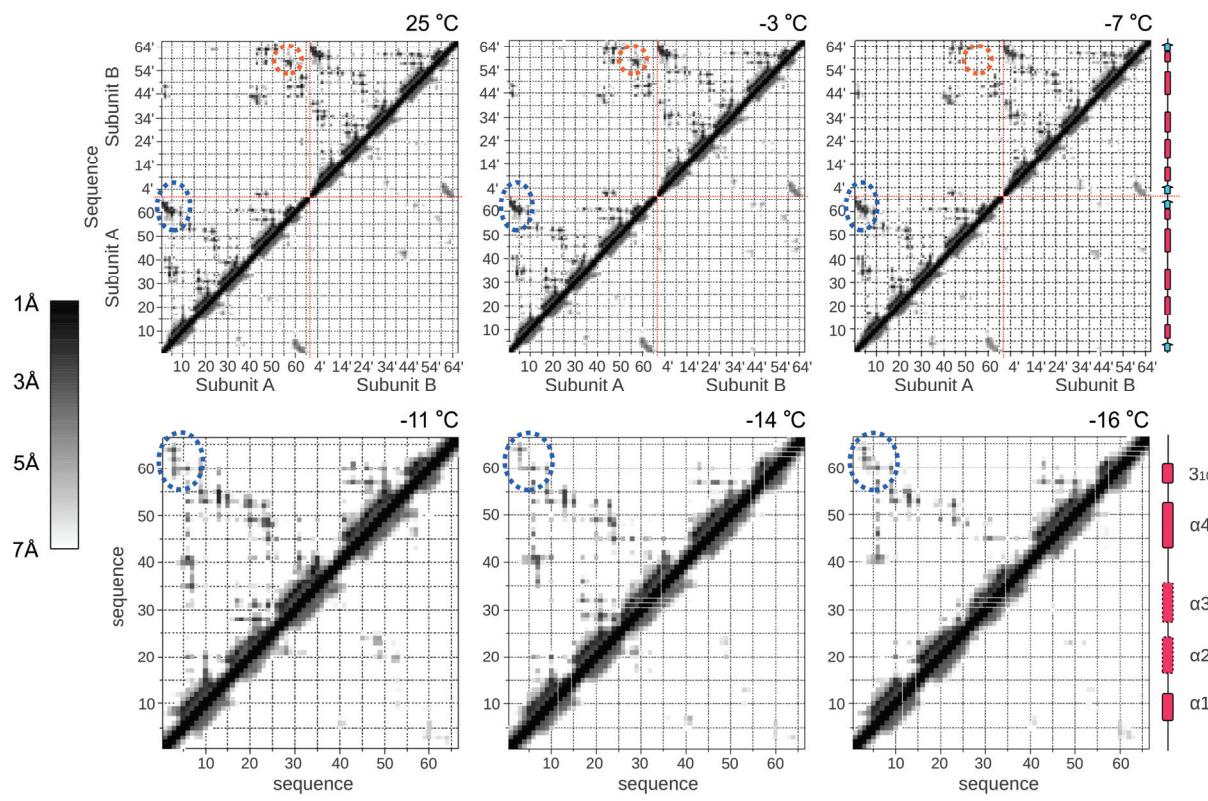
Supplementary Fig. 5. Contacts plots of CylR2 structures at different temperatures. The upper-left and lower-right parts indicate inter-proton and inter-heavy atom contacts, respectively. The three upper panels present the dimeric and the three lower panels the monomeric species. Secondary motifs are depicted on the right edge of the panel row. Red dashed circles highlight the symmetrical inter-subunit interactions between Pro56Leu57Glu58 fragments, which disappear at -7°C. The blue dashed circle marks the hydrophobic interactions between the C- and N-terminal parts of CylR2 that partially remain despite the loss of the four H-bonds stabilizing the anti-parallel β-strands of CylR2.
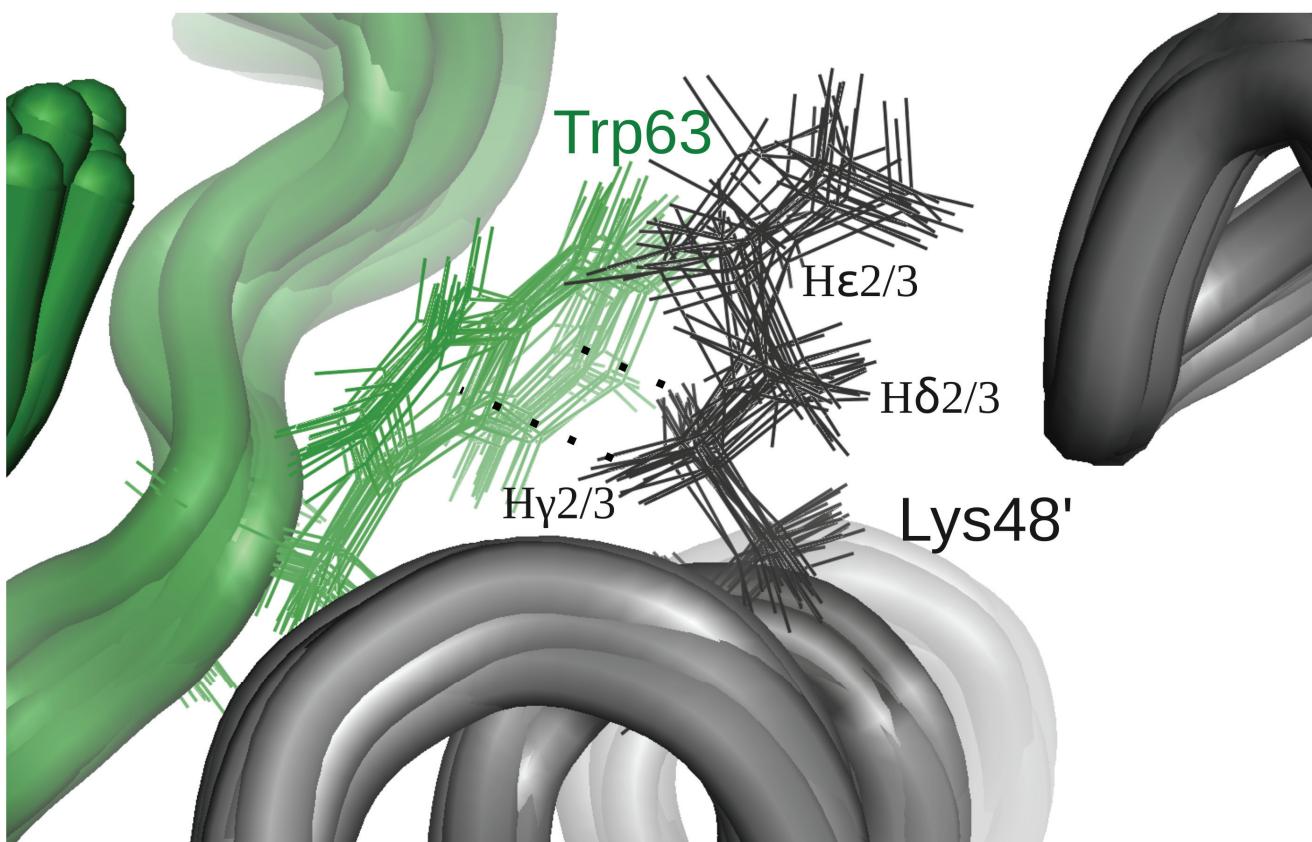
Supplementary Fig. 6. Expanded small region of the NMR ensemble of CylR2 at 25 °C highlighting the intermolecular C-H···π interaction between the aromatic moiety of Trp63 and the Hγ2/3 side chain protons of Lys48. The black dotted line is drawn from the side chain proton of Lys48 in subunit 1 (black) to the center of the aromatic moiety of Trp63 in subunit 2 (green).
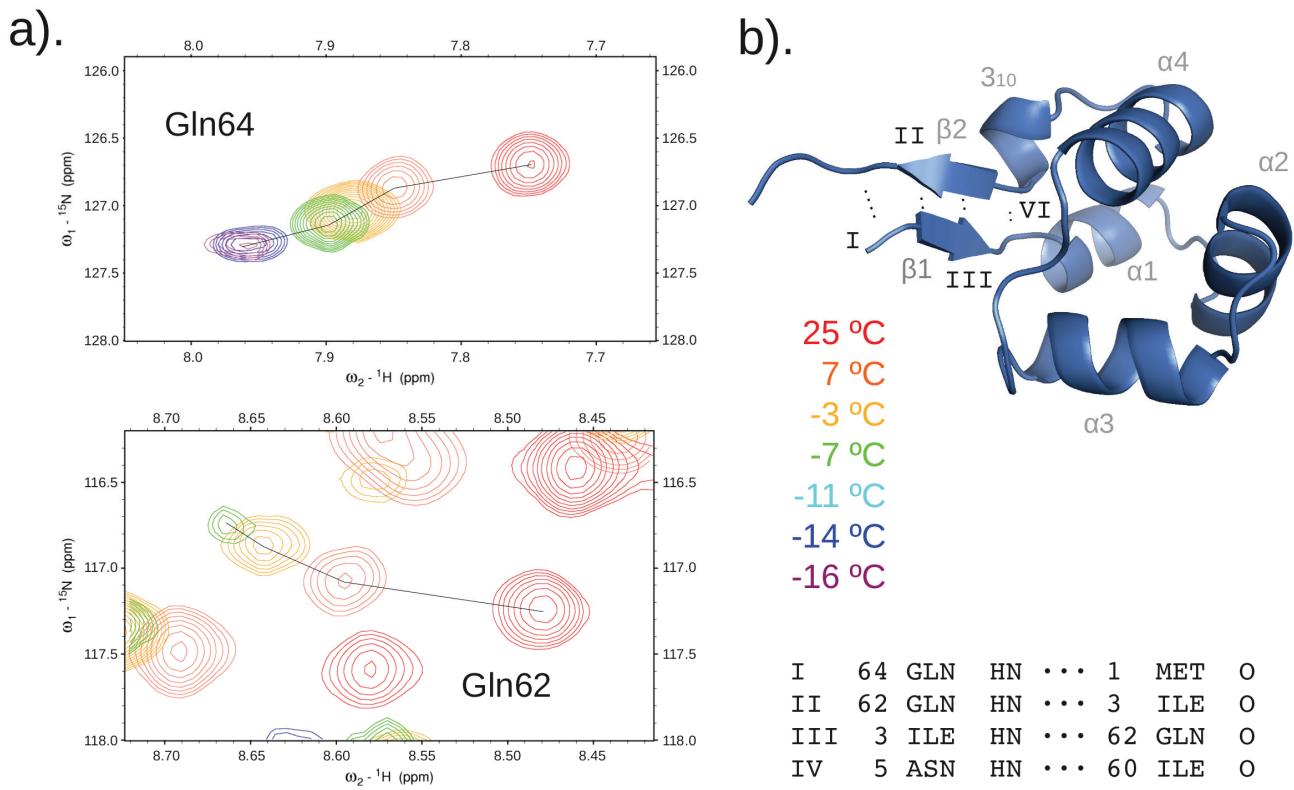
Supplementary Fig. 7. (a) Selected regions from 2D [^{1}H,^{15}N] HSQC spectra at different temperatures highlighting the non-linear temperature dependence of amide protons of Gln62 and Gln42. (b) H-bonds that stabilize the N and C-terminal β-strands at the temperatures above -7 °C.
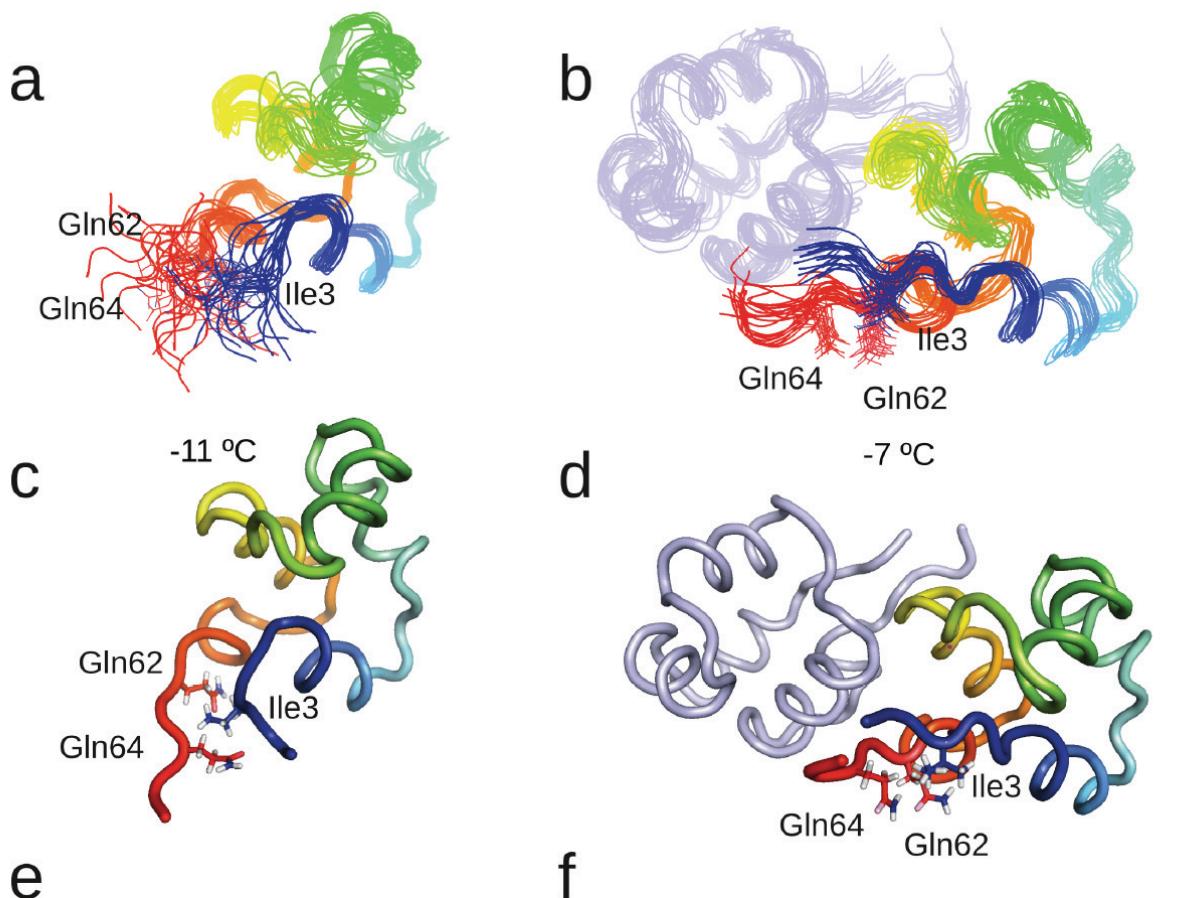
Supplementary Fig. 8. Mechanism of unfolding of the intramolecular β-sheet of CylR2. Backbone representations of the NOE-based structures of CylR2 determined at -11 °C **(a and c)** and at -7 °C **(b and d)**. The side chains of residues that keep the native contacts between the two antiparallel β-strands in the predissociated dimer (structure at -7 °C) and in the monomeric intermediate (structure at -11 °C) are drawn as sticks. **(e)** and **(f)** highlight specific contacts between these residues observed in 3D ^{13}C-edited NOESY-HSQC spectra at -11 °C and -7 °C, respectively. Despite the strong destabilization of the backbone of the β-sheet native-like contacts of the side chains.
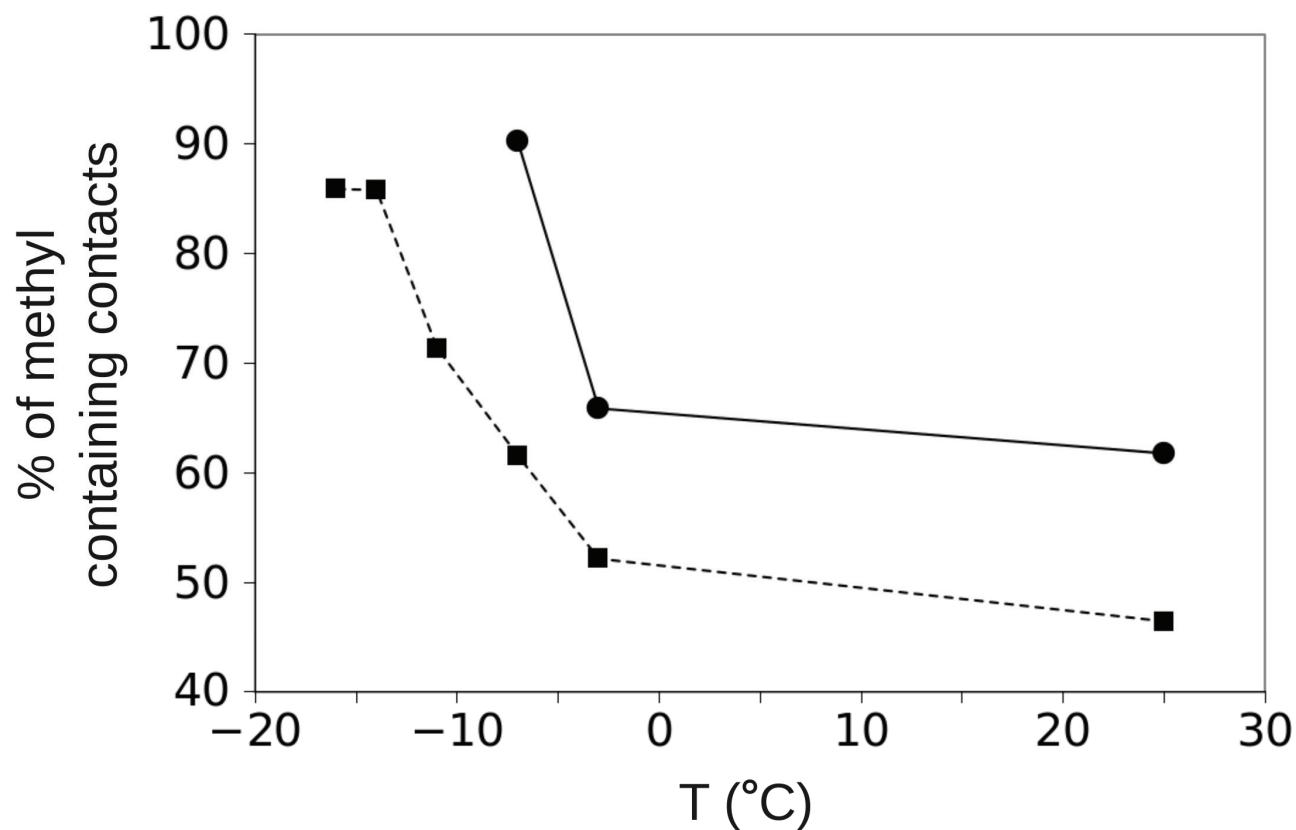
Supplementary Fig. 9. Fraction of methyl-containing NOE contacts at different temperatures within a CylR2 monomer (dashed line) and between the two molecules of the CylR2 dimer (solid line).
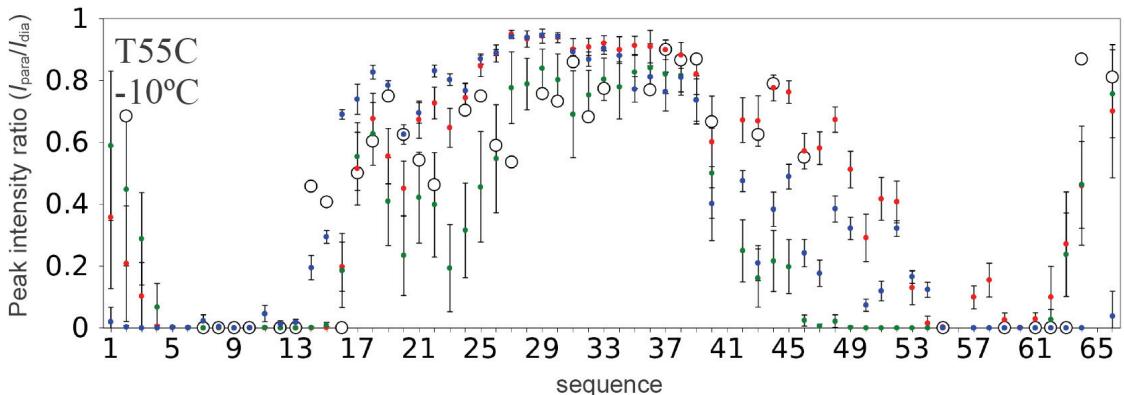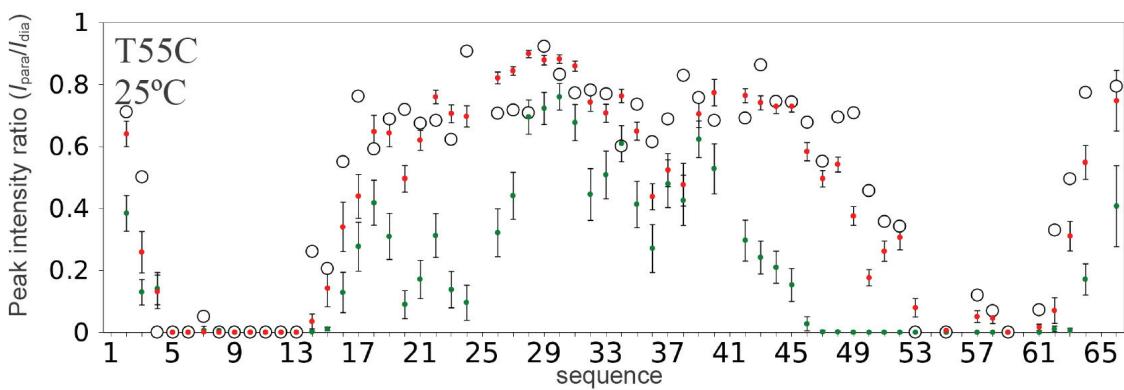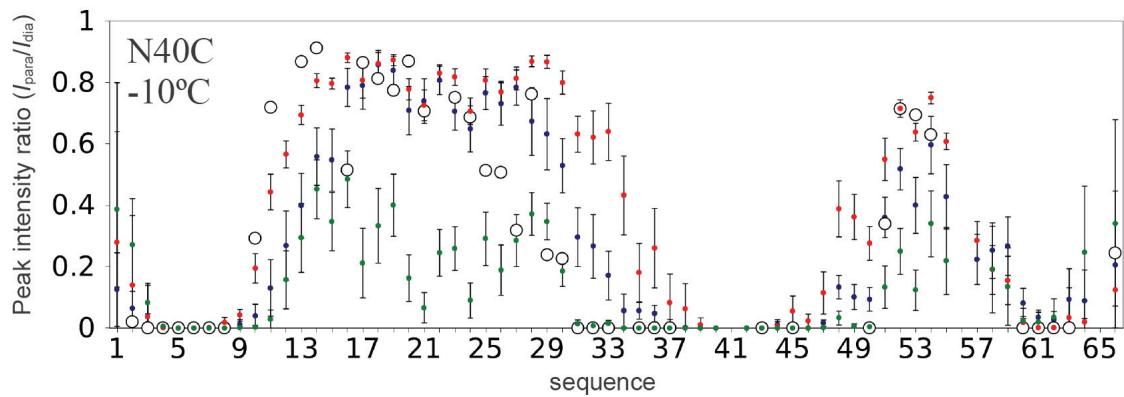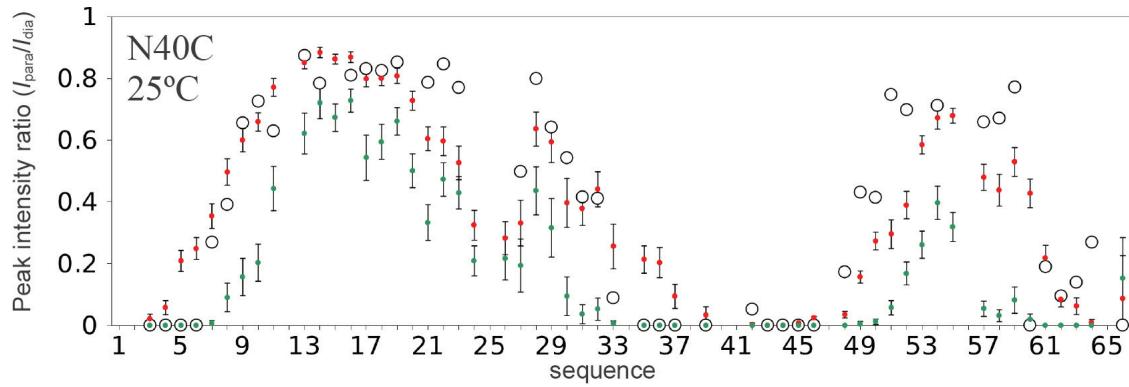
Supplementary Fig. 10. Comparison of experimental PRE profiles with values predicted from 3D structures of CylR2 during cold-denaturation. In the upper two panels results for N40C MTSL-tagged CylR2 are shown. In the lower two panels the results for T55C MTSL-tagged CylR2 are presented. Experimental PRE profiles are shown as open circles and were recorded at 25 °C and -10 °C. Green points mark the theoretical profiles predicted by positioning the paramagnetic center at the Cβ atom of N40 (upper two panels) and T55 (lower two panels). The red profiles were predicted when the paramagnetic center was located at the oxygen of a MTSL molecule that was attached to cysteine 40 and 55, respectively. Blue profiles are from MTSL positions rotated by ~180° around the S-S bond between cysteine and MTSL. Error bars for predicted profiles represent ± 1 standard deviation from the linear average of 20 predicted profiles within the ensemble of 20 conformers at each temperature. Averaged errors from three measurements for experimental PRE intensities are 0.11 for N40C at -10 ^{o}C, 0.10 for N40C at 25 ^{o}C, 0.08 for T55 at -10 ^{o}C and 0.06 for T55C at 25 ^{o}C. The comparison of the experimental PRE data with predicted values highlights the impact of the exact position of the paramagnetic center and therefore the conformation of the MTSL side chain for prediction of PRE values from a 3D structure.
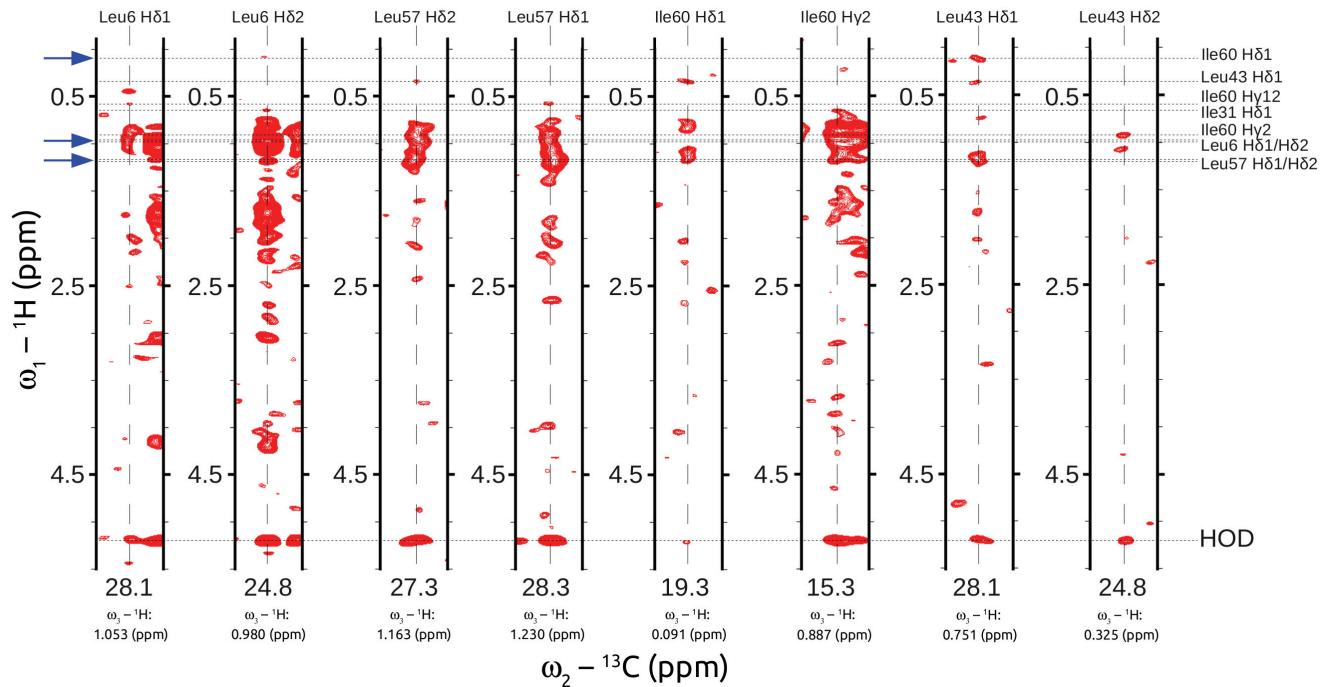
Supplementary Fig. 11. Strips from the 3D ^{13}C-edited NOESY-HSQC spectrum at -11 °C demonstrating the presence of non-native contacts between Ile60, Leu57, Leu43 and Leu6 (indicated by blue arrows) in the monomeric intermediate.

a).

b).

c).

K48 Hδ2/Hδ2

d).

e).

f).
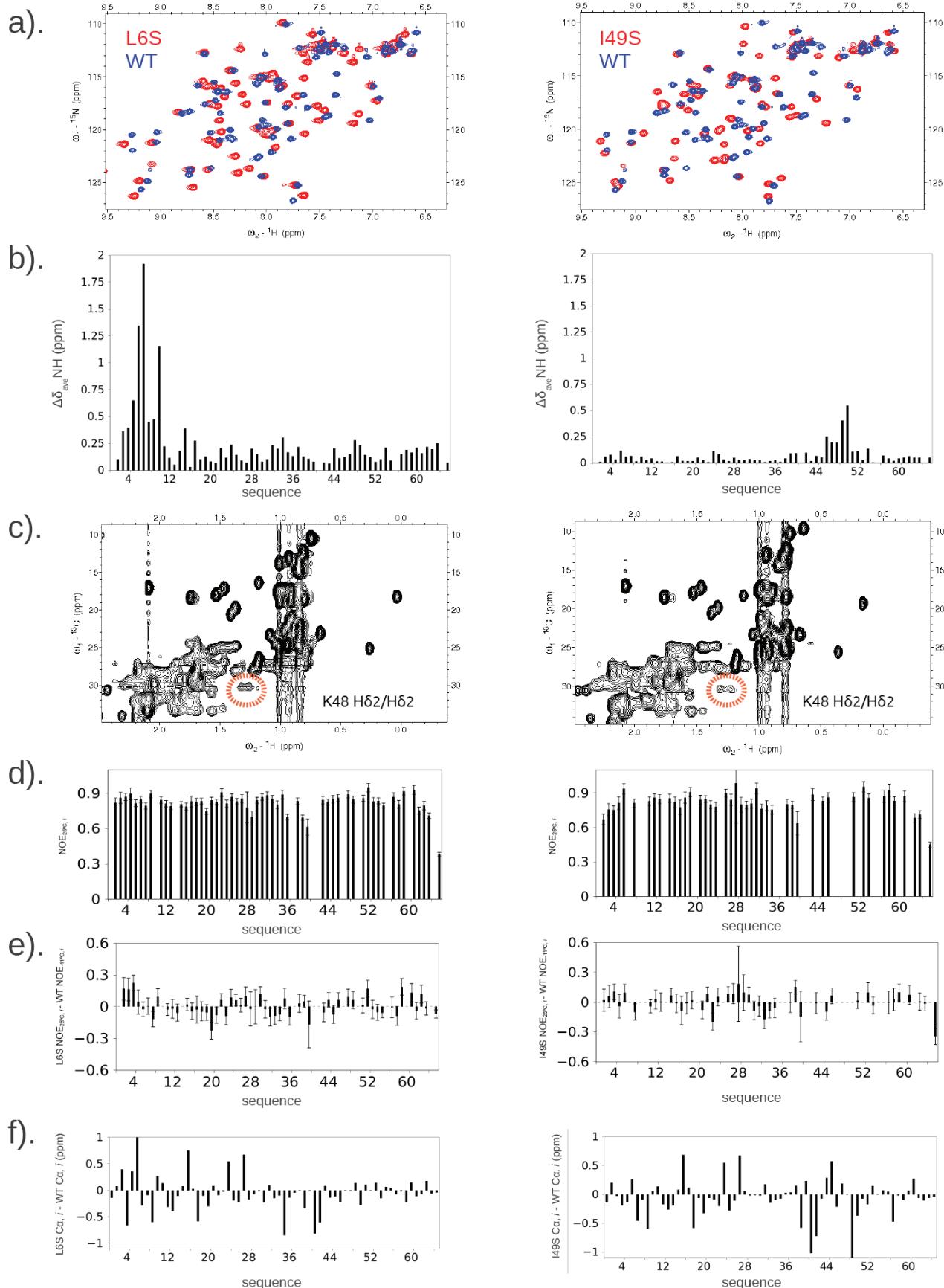
Supplementary Fig. 12. Effect of the point mutations L6S (left column) and I49S (right column) on CylR2. (a) Superposition of 2D [^{1}H,^{15}N] HSQC spectra for mutant (red) and wild-type (WT) protein (blue). (b) Normalized and averaged ^{1}H/^{15}N chemical shift differences of backbone amide resonances in mutant CylR2 with respect to the wild-type form. The error in $\Delta\delta$ is 0.05 ppm. (c) 2D [^{1}H,^{13}C] NOESY planes of L6S and I49S mutant CylR2 highlighting the strongly shifted side chain chemical shifts of the K48 side chain due to the presence of intersubunit C-H⋯π interactions between the aromatic moiety of Trp63 and the Lys48 side chain. (d) Steady-state ^{15}N-^{1}H NOE values at 25 °C for mutants and (e) their difference plots against wild-type CylR2. f) Difference plots between Cα chemical shifts of mutant and wild-type CylR2. The secondary motifs are preserved in both mutants. The maximum error is 0.2 ppm.
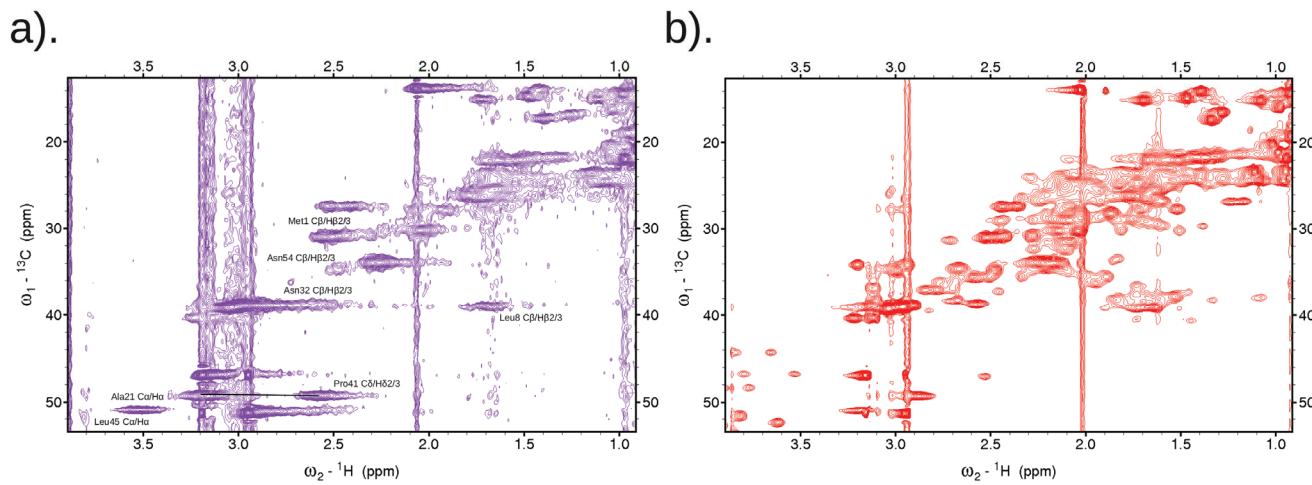
Supplementary Fig. 13. Selected region of 2D [^{1}H,^{13}C] HSQC spectra of cylR2 at -16 °C (a) and 25 °C (b). Selected Cα/Hα and side chain resonances are labelled.
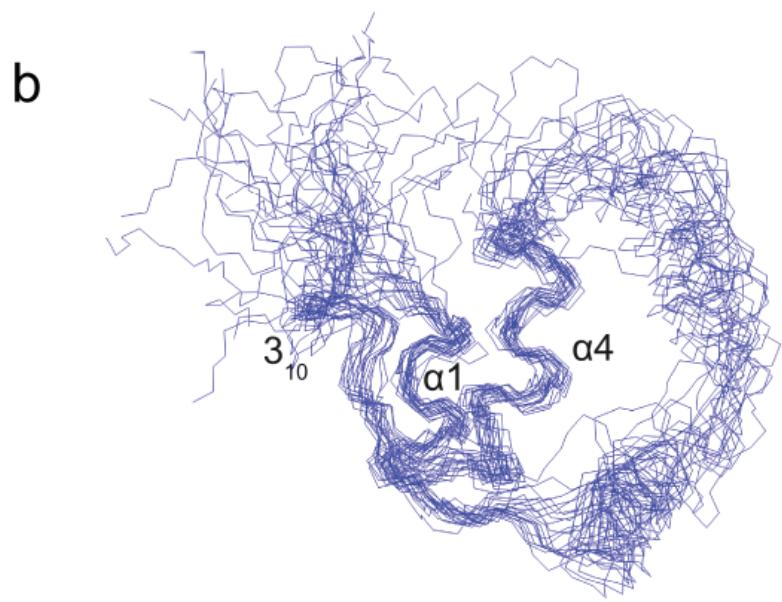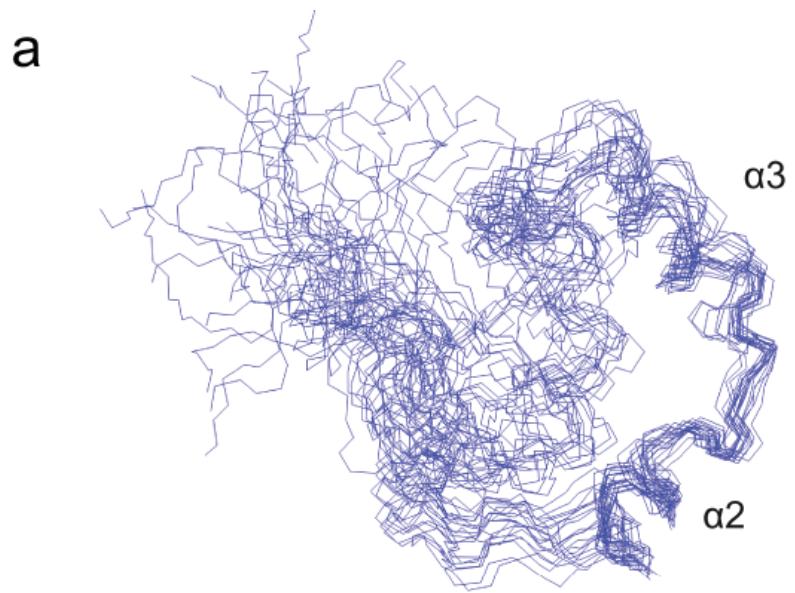
Supplementary Fig. 14. Ensemble of conformers of the partially folded monomeric intermediate at -16 °C using different subdomains for superposition. **(a)** The helix-turn-helix motif was used for alignment. **(b)** Helices $\alpha 1$, $\alpha 4$ and 3_{10} were used for alignment.
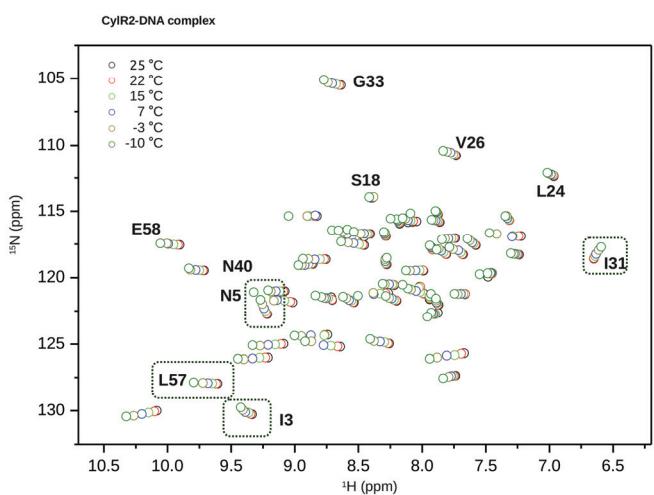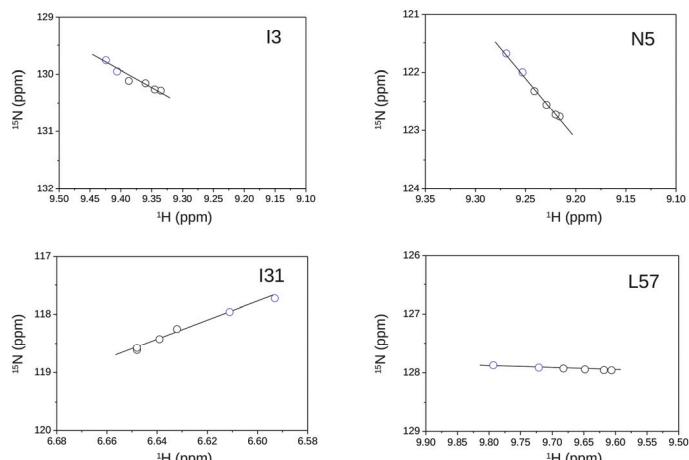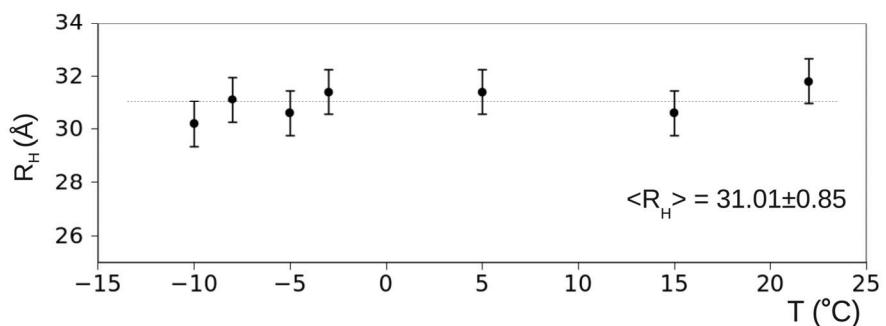
Supplementary Fig 15. Temperature dependence of the CylR2-DNA complex. a) 2D [^{1}H,^{15}N] TROSY-HSQC spectra as a function of temperature. b) 2D chemical shift plots for selected residues demonstrating a linear chemical shift dependence for decreasing temperature. c) Hydrodynamic radius (R_h) as a function of temperature. The averaged hydrodynamic radius (dotted line) $\langle R_h \rangle$ = 31.01±0.85 Å of the CylR2-DNA complex remains unchanged along the studied temperature range within the experimental error.
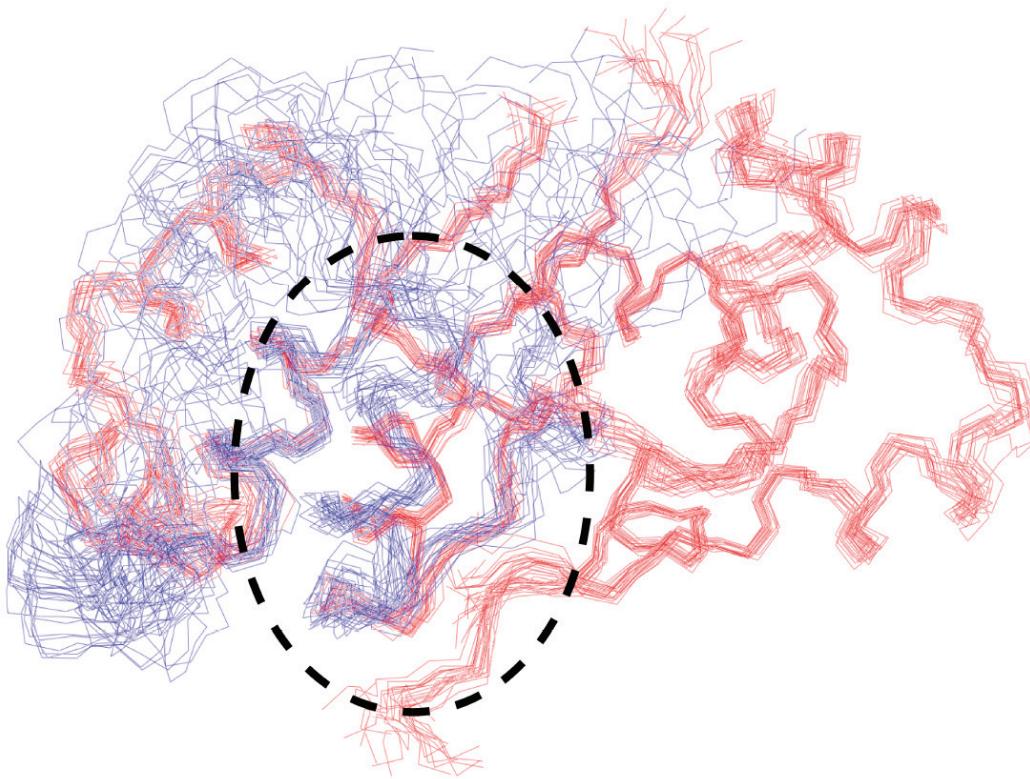
Supplementary Fig 16. The core of the partially folded intermediate forms the dimer interface in the native state. Superposition of the NOE-based ensemble of conformers at -16 °C (blue) and the native CylR2 dimer determined at 25 °C (red). The superimposed fragments consist of Leu6 - Ile15 and Leu43 - Ile60 marked by an ellipse. The two α-helices (α1 and α4) and one 3_{10}-helix form the folding nucleus that predisposes the protein for dimerization.

Supplementary Table 1 | Simulation of the effect of changes in the global correlation time (tau_c) and in the time scale (tau_i) and amplitude (S^2) of internal motions on ^{15}N-^{1}H NOE values. Changes in global correlation time are due to the temperature-dependence of solution viscosity (increase from 25 °C to 5 °C) and due to the dissociation of the CylR2 dimer into a monomer at -11 °C. Calculations have been done using Lipari-Szabo's correlation functions assuming a nearly isotropic global motion and fast internal motions that are separable from global motion [2,3].

T (°C)	tau-c (ns)	tau-i (ps)	S^2	^{15}N-^{1}H NOE	sigma (s^{-1})	R_1 (s^{-1})	R_2 (s^{-1})
25	12	20	0.85	0.76	0.017	0.72	17.78
5	22	20	0.85	0.69	0.013	0.41	32.13
-11	16	20	0.85	0.73	0.015	0.55	23.50
-11	16	20	0.52	0.27	0.029	0.40	14.42
-11	16	150	0.85	0.28	0.048	0.66	23.59
-11	16	45	0.7	0.27	0.039	0.54	19.42

Supplementary Table 2 | List of NMR experiments.

List of experiments at different temperatures	TD			SW (Hz)			NS
	F1	F2	F3	F1	F2	F3	
25°C							
2D [^{1}H, ^{15}N] HSQC	2048	128	–	9803.992	1421.262	–	16
2D [^{1}H, ^{15}N] HSQC	2048	128	–	9803.992	1421.262	–	32
2D ^{15}N–^{1}H Het-NOE	2048	128	–	9803.992	1421.262	–	40
2D [^{1}H, ^{13}C] HSQC ali	2048	128	–	9803.992	13054.83	–	16
2D [^{1}H, ^{13}C] HSQC aro	2048	50	–	8417.508	5291.005	–	16
3D ^{15}N-edited NOESY-HSQC (150ms)	2048	210	50	9090.909	9115.77	1421.262	8
3D ^{13}C-edited NOESY-HSQC ali (200 ms)	2048	50	230	9090.909	7052.186	9115.77	8
3D ^{13}C-edited NOESY-HSQC aro (200 ms)	2048	40	196	9090.909	4585.053	9115.77	8
3D CCH TOCSY	2048	120	64	7716.049	13054.83	13054.83	8
7°C							
2D [^{1}H, ^{15}N] HSQC	2048	128	–	9803.992	1421.262	–	16
–3°C							
2D [^{1}H, ^{15}N] HSQC	2048	128	–	9803.992	1421.262	–	16
2D [^{1}H, ^{15}N] HSQC	2048	128	–	9803.992	1421.262	–	32
2D ^{15}N–^{1}H Het-NOE	2048	128	–	9803.992	1421.262	–	50
2D [^{1}H, ^{13}C] HSQC ali	2048	128	–	8417.508	13054.83	–	16
2D [^{1}H, ^{13}C] HSQC aro	2048	50	–	8417.508	5291.005	–	16
3D ^{15}N-edited NOESY-HSQC (150ms)	2048	210	50	9090.909	9115.77	1421.262	16
3D ^{13}C-edited NOESY-HSQC ali (200 ms)	2048	50	230	9090.909	7052.186	9115.77	16
3D ^{13}C-edited NOESY-HSQC aro (200 ms)	2048	40	196	9090.909	4585.053	9115.77	16
3D CCH TOCSY	2048	120	64	7716.049	13054.83	13054.83	8
–7°C							
2D [^{1}H, ^{15}N] HSQC	2048	128	–	9803.992	1421.262	–	32
2D [^{1}H, ^{13}C] HSQC ali	2048	128	–	8417.508	13054.83	–	32
2D [^{1}H, ^{13}C] HSQC aro	2048	50	–	8417.508	5291.005	–	32
3D ^{15}N-edited NOESY-HSQC	2048	46	230	7716.049	7052.186	7716.049	32
3D ^{13}C-edited NOESY-HSQC ali (200 ms)	2048	50	230	9090.909	7052.186	9115.77	16
3D ^{13}C-edited NOESY-HSQC aro (200 ms)	2048	50	196	9090.909	4585.053	9115.77	16
3D CCH TOCSY	2048	120	64	7716.049	13054.83	13054.83	8
–11°C							
2D [^{1}H, ^{15}N] HSQC	2048	128	–	9803.992	1421.262	–	64
2D [^{1}H, ^{15}N] HSQC	2048	128	–	9803.992	1421.262	–	32
2D ^{15}N–^{1}H Het-NOE	2048	100	–	9803.992	1421.262	–	400
2D [^{1}H, ^{13}C] HSQC ali	2048	112	–	8417.508	13054.83	–	64
2D [^{1}H, ^{13}C] HSQC aro	2048	50	–	8417.508	5291.005	–	64
3D ^{15}N-edited NOESY-HSQC	2048	46	230	7716.049	7052.186	7716.049	32
3D ^{13}C-edited NOESY-HSQC ali (200 ms)	2048	50	230	9090.909	7052.186	9115.77	16

3D CCH TOCSY	2048	120	64	7716.049	13054.83	16	
−14°C							
2D [^{1}H, ^{15}N] HSQC	2048	128	−	9803.992	1421.262	−	64
2D [^{1}H, ^{15}N] HSQC	2048	128	−	9803.992	1421.262	−	32
2D [^{1}H, ^{13}C] HSQC ali	2048	128	−	8417.508	13054.83	−	64
2D [^{1}H, ^{13}C] HSQC aro	2048	50	−	8417.508	5291.005	−	64
3D ^{13}C-edited NOESY-HSQC ali (200 ms)	2048	50	230	9090.909	7052.186	9115.77	32
3D ^{13}C-edited NOESY-HSQC aro (200 ms)	2048	50	196	9090.909	4585.053	9115.77	16
3D CCH TOCSY	2048	120	64	7716.049	13054.83	13054.83	16
−16°C							
2D [^{1}H, ^{15}N] HSQC	2048	128	−	9803.992	1421.262	−	64
2D [^{1}H, ^{15}N] HSQC	2048	128	−	9803.992	1421.262	−	32
2D [^{1}H, ^{13}C] HSQC ali	2048	128	−	8417.508	13054.83	−	64
2D [^{1}H, ^{13}C] HSQC aro	2048	40	−	8417.508	5291.005	−	64
3D ^{13}C-edited NOESY-HSQC ali (200 ms)	2048	50	230	9090.909	7052.186	9115.77	32
3D CCH TOCSY	2048	120	64	7716.049	13054.83	13054.83	16
Mutant L6S at 25°C							
2D [^{1}H, ^{15}N] HSQC	2048	128	−	9803.992	1421.262	−	16
2D [^{1}H, ^{13}C] HSQC ali	2048	128	−	8417.508	13054.83	−	32
2D ^{15}N–^{1}H Het-NOE	2048	128	−	9803.992	1421.262	−	40
3D ^{13}C-edited NOESY-HSQC ali (200 ms)	2048	50	1	9090.909	7052.186	9115.77	16
3D NHCACB	2048	50	100	9803.922	1421.264	13227.51	16
3D HNCA	2048	50	60	9803.922	1421.262	4938.272	16
3D CBCAcoNH	2048	50	100	9803.922	1421.262	13227.51	16
Mutant I49S at 25°C							
2D [^{1}H, ^{15}N] HSQC	2048	128	−	9803.992	1421.262	−	16
2D [^{1}H, ^{13}C] HSQC ali	2048	128	−	8417.508	13054.83	−	32
2D ^{15}N–^{1}H Het-NOE	2048	128	−	9803.992	1421.262	−	40
3D ^{13}C-edited NOESY-HSQC ali (200 ms)	2048	50	1	9090.909	7052.186	9115.77	16
3D HNCA	2048	50	60	9803.922	1421.262	4938.272	16
3D CBCAcoNH	2048	50	100	9803.922	1421.262	13227.51	16

Supplementary Table 3 | NMR and refinement statistics for protein structures

	-16 °C	-14 °C	-11 °C	-7 °C[a]	-7 °C[a]	-3 °C	25 °C
NMR distance and dihedral constraints (per subunit)							
Distance constraints							
Total NOE	168	249	610	1045	1096	1580	1757
Intra-residue	47	69	121	268	268	365	457
Inter-residue	121	180	489	777	777	1215	1300
Sequential ($|i-j|=1$)	22	39	129	232	232	368	413
Medium-range ($|i-j|<4$)	35	56	170	261	261	344	369
Long-range ($|i-j|>5$)	64	85	190	284	284	412	416
Intermolecular	-	-	-	-	51	91	102
Hydrogen bonds	-	-	-	-	-	-	-
Total dihedral angle restraints							
φ	**48**	**48**	**48**	**48**	**48**	**56**	**56**
ψ	**48**	**48**	**48**	**48**	**48**	**56**	**56**
Structure statistics[b]							
Violations (mean and s.d.)							
Distance constraints (Å)	0.053±0.008	0.043±0.004	0.045±0.005	0.040±0.004	0.038±0.004	0.025±0.002	0.027±0.001
Dihedral angle constraints (°)	0.852±0.279	0.675±0.138	0.788±0.131	0.305±0.089	0.318±0.082	0.373±0.062	0.420±0.051
Max. dihedral angle violation (°)	3.768±0.719	4.032±0.707	4.091±0.426	2.205±0.867	2.805±0.549	3.234±0.728	3.261±0.827
Max. distance constraint violation (Å)	0.291±0.058	0.253±0.033	0.363±0.044	0.405±0.041	0.419±0.044	0.333±0.144	0.402±0.044
Deviations from idealized geometry							
Bond lengths (Å) · 10^{-3}	1.900±0.077	1.440±0.045	2.971±0.027	1.986±0.015	1.779±0.014	1.297±0.008	1.314±0.041
Bond angles (°)	0.449±0.011	0.382±0.002	0.526±0.002	0.411±0.001	0.408±0.001	0.374±0.001	0.378±0.001
Impropers (°)	0.332±0.033	0.225±0.001	0.355±0.002	0.255±0.001	0.249±0.002	0.216±0.002	0.221±0.001
Average pairwise r.m.s. deviation (Å)							
Heavy	3.14±0.74	2.34±0.34	1.73±0.24	1.47±0.18	1.30±0.14	1.04±0.09	0.97±0.08
Backbone	2.17±0.52	1.52±0.26	1.08±0.27	0.75±0.13	0.70±0.11	0.55±0.07	0.50±0.07
Ramachandran Plot Statistics							
residues in most favoured (%)	83.7	83.5	81.4	84.5	86.9	94.6	96.5
residues in additional allowed (%)	14.1	14.1	13.8	11.5	10.3	4.2	2.5
residues in generously allowed (%)	1.3	1.7	2.0	3.3	2.2	0.9	1.0
residues in disallowed (%)	0.9	0.8	2.8	0.8	0.7	0.3	0.0

a) For the ensemble calculations at -7 C°, which used an equal mixture of dimeric and monomeric forms, XPLOR-NIH was modified.

b) Evaluated for 20 lowest energy structures out of a total 200 calculated structures.

Supplementary Table 4 | Distances averaged for conformers of CylR2 ensembles determined at different temperatures.

Temperature (°C)	**Distances (Å; ave±sdev)**					
	Cγ – Cζ'	**Cα – Cα**				
	P65-Y51'	**L57-L57'**	**L6-I60**	**L6-I49**	**L6-I31**	**L6-L24**
25	4.0 ± 0.4	7.1 ± 0.3	5.1 ± 0.1	8.2 ± 0.1	8.9 ± 0.3	12.9 ± 0.5
-3	8.8 ± 1.1	6.7 ± 0.4	5.2 ± 0.2	8.0 ± 0.2	9.0 ± 0.3	13.1± 0.7
-7 (dimer)	11.9 ± 2.1	10.2 ± 0.9	4.4 ± 0.3	8.6 ± 0.3	8.8 ± 0.4	13.1 ± 0.5
-7 (monomer)	N/A	N/A	4.9 ± 0.6	8.7 ± 0.3	8.7 ± 0.3	12.9 ± 0.4
-11	N/A	N/A	6.4 ± 0.4	9.7 ± 0.4	11.9 ± 1.0	13.2 ± 0.7
-14	N/A	N/A	6.8 ± 0.6	11.0 ± 0.9	16.4 ± 1.2	16.4 ± 0.9
-16	N/A	N/A	7.0 ± 0.6	9.7 ± 1.0	14.0 ± 1.4	15.5 ± 1.1

Supplementary Video 1 – Structural changes that occur during cold-induced unfolding of CylR2 at atomic resolution. Each frame shows a single structure taken from the ensembles of 20 lowest-energy NOE-based structures determined at 25 °C, -3 °C, -7 °C, -11 °C, -14 °C and -16 °C, respectively. For the majority of residues only back-bone heavy atoms are presented. For residues crucial for both tertiary and quaternary folding side chains are also shown.

1. Hallett, J. Temperature Dependence of Viscosity of Supercooled Water. *P Phys Soc Lond* **82**, 1046-1050 (1963).
2. Lipari, G. & Szabo, A. Model-Free Approach to the Interpretation of Nuclear Magnetic-Resonance Relaxation in Macromolecules .1. Theory and Range of Validity. *J Am Chem Soc* **104**, 4546-4559 (1982).
3. Palmer, A.G., 3rd NMR characterization of the dynamics of biomacromolecules. *Chem Rev* **104**, 3623-3640 (2004).